The Effect of Low-Vacuum Environments on Particulate Contamination near Starshade Edges

Brandon J. Titensor[a], Lauren W. Miner[a], Joshua J. Vawdrey*[a], Stuart B. Shaklan[b], and David D. Allred[a]

[a]Brigham Young University, Department of Physics and Astronomy, Provo, Utah 84604
[b]Jet Propulsion Laboratory, California Institute of Technology, Pasadena, California 91109

ABSTRACT

Starshade technology represents a promising approach for direct exoplanet imaging, offering stellar light suppression up to a factor of 10^{10}. Particulate contamination that clings to the edge of the starshade causes solar glint which could compromise Earth-like exoplanet detection. In previous research, when testing at atmospheric pressure, McKeithen et al. 2023 observed that the sharp edge have fewer particles larger than 14 microns, and more particles smaller than 14 microns, than expected from the surface distribution.[1] To determine if this observation was reproducible in different environments, we contaminated starshade edge coupons in low vacuum conditions. We characterized the surface and edge cleanliness level using optical microscopy, a custom ImageJ macro and R program that calculated the counts and area of particles in each image. We then compared our results with McKeithen et al. confirming their result, but the crossover occurred at particle diameters of about 3 microns rather than 14 microns. In our work, we propose different mechanisms which could affect any differences between the vacuum environment tests and the tests performed in air previously.

Keywords: Contamination, Dust, Habitable Worlds Observatory, HWO, Starshade, Technology, Edge Contamination, Surface Contamination

1. INTRODUCTION

Contamination control on starshades is necessary to prevent solar glint off dust particulates from ruining earth-like exoplanet detection. It has been calculated that approximately 1 mm^2 coverage of particulates on a 10 m segment of the starshade edge can cause solar scattering equivalent to the brightness of an Earth-like exoplanet .[1]

Contamination can be categorized by particulate or molecular contamination. For the purposes of this study, particulate contamination refers to any contaminant greater than or equal to 1 µm. While submicron particulates may be a concern, we assume that they will not be significant. Molecular contaminants are molecular layers (adventitious carbons, fingerprint oils, etc.).

To categorize how clean surfaces are, the Institute of Environmental Sciences and Technology (IEST) devised a series of standards for contamination control engineers to use. The IEST-STD-CC1246E standards give a cleanliness level based on the distribution of particulate contamination that may lie on the surface of the samples. However, as shown in McKeithen et al., the standards are designed for surfaces and not for edges.[1] The cleanliness of edges, therefore, needs to be considered in deeper detail. McKeithen et al found that an "adhesion factor" proportional to the inverse diameter of the particles accounted for their observations of more small particles, and fewer large particles, than predicted by a line drawn across a contaminated surface.

The mechanism of the difference between the observed and predicted edge distributions was speculated to be electrostatic. Our work performs the contamination experiments in a vacuum. While McKeithen speculated that the need for an adhesion factor may be due to electrostatic effects, in vacuum we can explore whether the charge accumulated on the dust while in air, and potentially discriminate effects due to viscous flow.

Further author information: (Send correspondence to J.J.V.)
J.J.V.: E-mail: Joshua.J.Vawdrey@gmail.com, Telephone: +1(801)941-3781

Space Systems Contamination: Prediction, Control, and Performance 2025, edited by Carlos E. Soares, Bruce A. Matheson, Jillian Stack, Proc. of SPIE Vol. 13628, 1362802
2025 Published by SPIE · 0277-786X · doi: 10.1117/12.3065842

2. EXPERIMENTAL SET-UP

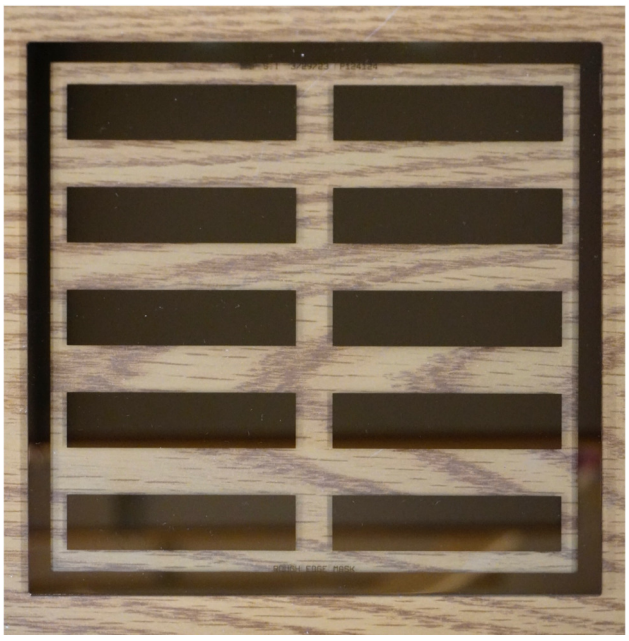
Our experiment is focused on repeating the McKeithen et al. experiment[1] in a low-vacuum environment. This requires:

1. Constructing a vacuum system capable of sustaining between 80 mTorr to 1000 mTorr during contamination
2. Analyzing each image corresponding to each sample for particulate contaminants
3. Predicting the edge contamination with the model from the McKeithen et al.[1] paper ("The Surface Line Model")

We compare the experimental results to a calibration wafer. The wafer is a sodalime glass with a chrome silhouette and edges matching the in-plane roughness of an edge coupon. (see Figure 2). The calibration wafer is intended to act like the "line on a surface" but with characteristics that will perform similarly to the starshade edge during image processing.



(a) Etched amorphous metal foil sample (38 µm thick)

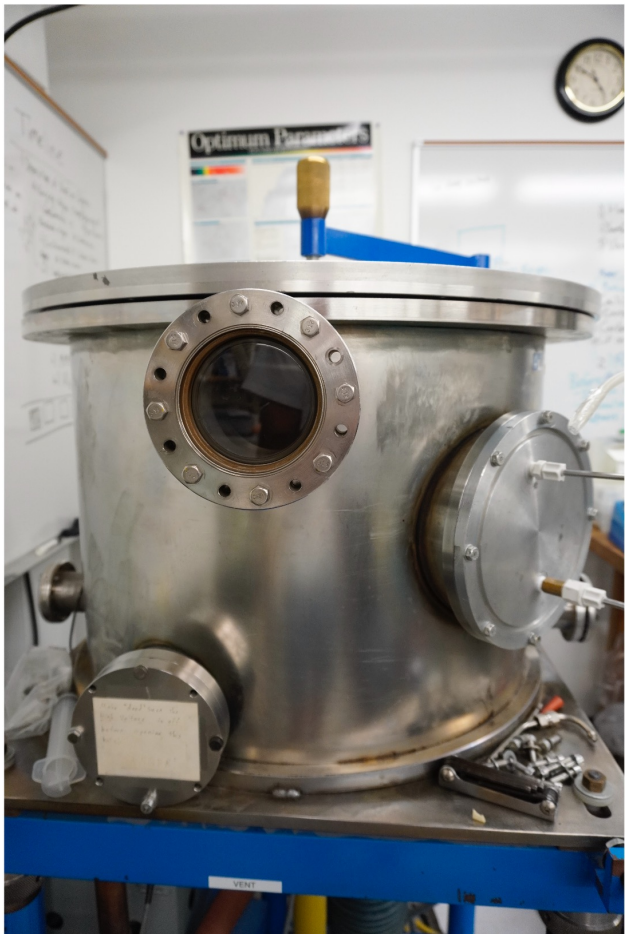


(b) Sodalime glass calibration mask with chrome edges

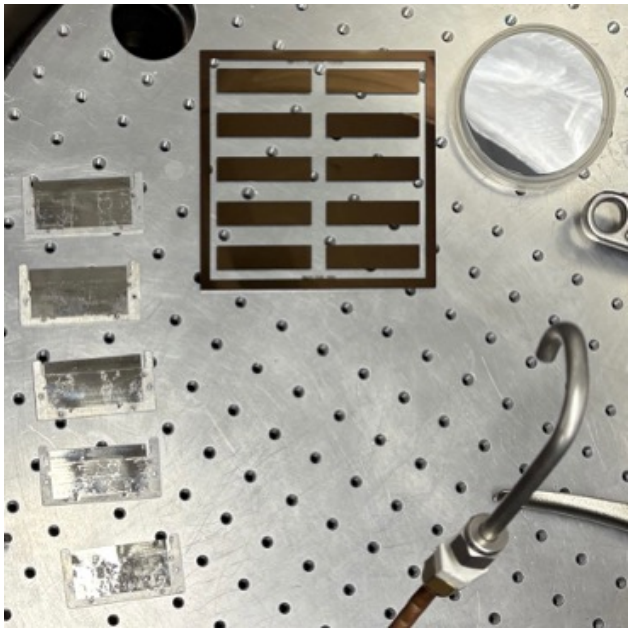
Figure 1: Test samples used for contamination experiments. (a) Starshade edge coupon from NASA-JPL. (b) Calibration mask with matching edge roughness used for model validation.

2.1 Contamination Trials

JPL delivered five starshade edge coupons for testing. We built a vacuum system designed specifically to contaminate starshade samples(See Fig. 3). As shown in Fig. 2b, the samples were placed near the dust source. Dust was deposited by "puffing" the dust into the chamber while the roughing pump was left on. After five seconds passed, the chamber was vented back to atmosphere. Once the system was at atmospheric pressure, the samples were removed and returned to their sample holders. The sample holders were transferred at a later date to a KEYENCE VHX-7000 microscope, where we performed a rastered scan of the surface and edge.



(a) Exterior of the custom vacuum system



(b) Interior of the vacuum system with samples

Figure 2: The vacuum chamber used to contaminate starshade edges. Inside view shows starshade samples and calibration mask positioned near the dust dispersion spout. Weights were used to hold down a narrow mesh to prevent particulates from getting into the diffusion pump.

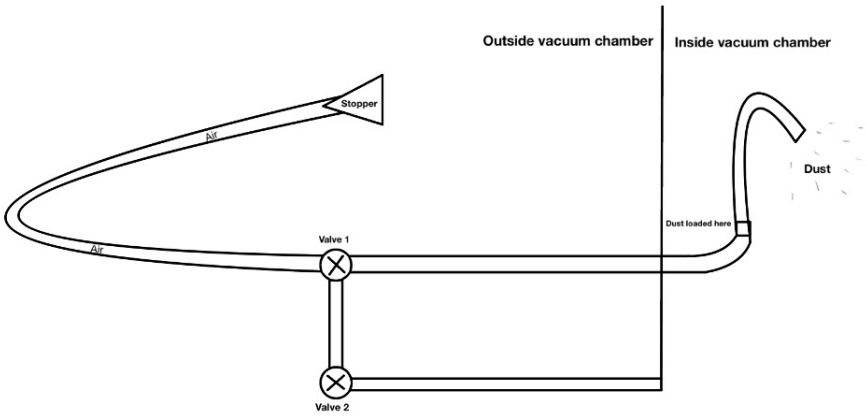


Figure 3: Diagram of the vacuum chamber system. As the system is pumped down, Valve 2 is opened. Once chamber is at 85 mTorr, valve 2 is shut, and valve 1 is opened for 5 s. This pushes air through the tube and disperses the dust. The tube was 41 cm long and and had a exterior diameter of 6.35 mm

3. IMAGE PROCESSING METHODOLOGY

3.1 Overview

FIJI (FIJI is an ImageJ bundle) was used to extract and quantify dust particulates from images captured by the KEYENCE VHX-7000 microscope across all experimental trials. Two distinct processing pipelines were developed: a simple approach for surface contamination analysis and a multi-step pipeline for edge contamination detection and qualification. Both methodologies incorporated automated brightness standardization to ensure consistent particle detection across temporal variations in imaging conditions.

3.2 Surface Image Processing

3.2.1 Brightness Normalization

Each surface image was subjected to a standardized brightness correction to compensate for temporal drift in illumination conditions between imaging sessions. The macro measured the original median brightness of each image and applied a linear transformation to center the median brightness at a target value, effectively removing variations in background illumination while preserving the relative intensity relationships important for threshold-based particle detection.

3.2.2 Particle Detection Parameters

Following brightness standardization, images were processed using the following standardized parameters:

- **Threshold range:** 72–255 (on 8 bit scale) to isolate particles from background
- **Scale calibration:** 0.2083 µm per 1 pixel
- **Binary conversion:** Images were converted to binary masks to clearly delineate particle boundaries

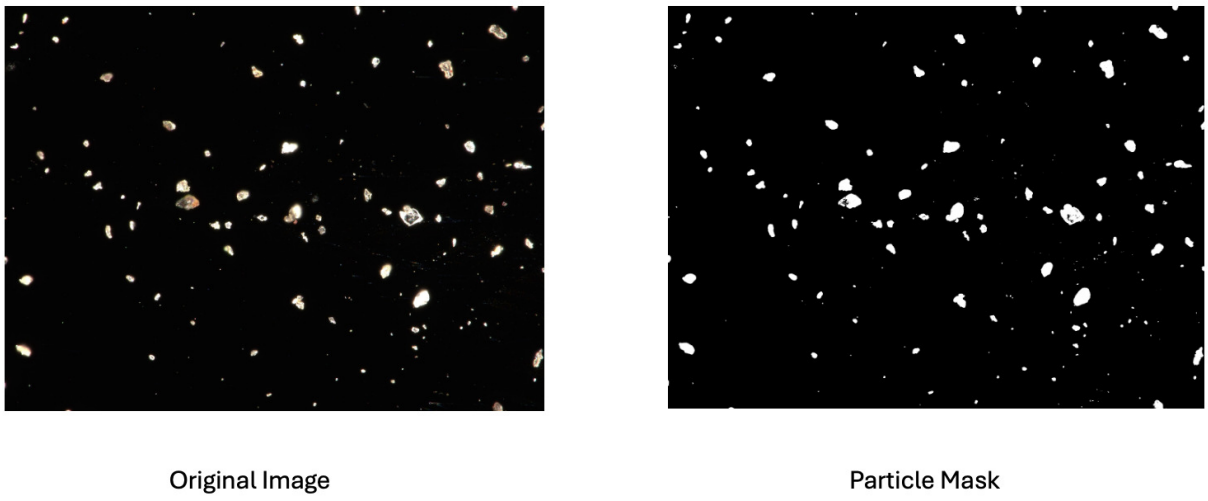


Figure 4: Image processing workflow for surface contamination analysis. Shows particle detection and quantification pipeline for surface measurements.

3.2.3 Automated Analysis

The macro executed ImageJ's "Analyze Particles" function on each processed image, automatically detecting, counting, and measuring particle areas. Measurements included particle area, centroid coordinates, bounding box dimensions, and shape descriptors. Results were exported as CSV files containing individual particle measurements and summary statistics for each image.

3.3 Edge Image Processing

Edge contamination presented unique analytical challenges requiring a more sophisticated processing approach than surface analysis. The primary difficulty was distinguishing newly deposited particles from existing edge features while accounting for minor positional variations between pre- and post-contamination imaging sessions.

3.3.1 Image Registration and Alignment

Edge contamination analysis required precise alignment of before and after contamination image pairs. Each edge sample was imaged at 500 × magnification using profile lighting to create high-contrast edge silhouettes. The processing pipeline performed the following registration steps:

1. **Descriptor-based registration:** The macro employed ImageJ's descriptor-based registration algorithm with rigid transformation model to align image pairs, compensating for minor positional shifts between imaging sessions
2. **Registration parameters:** Minima & maxima detection, 3D quadratic fit subpixel localization, 3 neighbors, redundancy factor of 2, significance threshold of 3, and 6 pixel RANSAC error tolerance
3. **Quality verification:** Registration success was validated by confirming creation of properly fused image pairs before proceeding with analysis

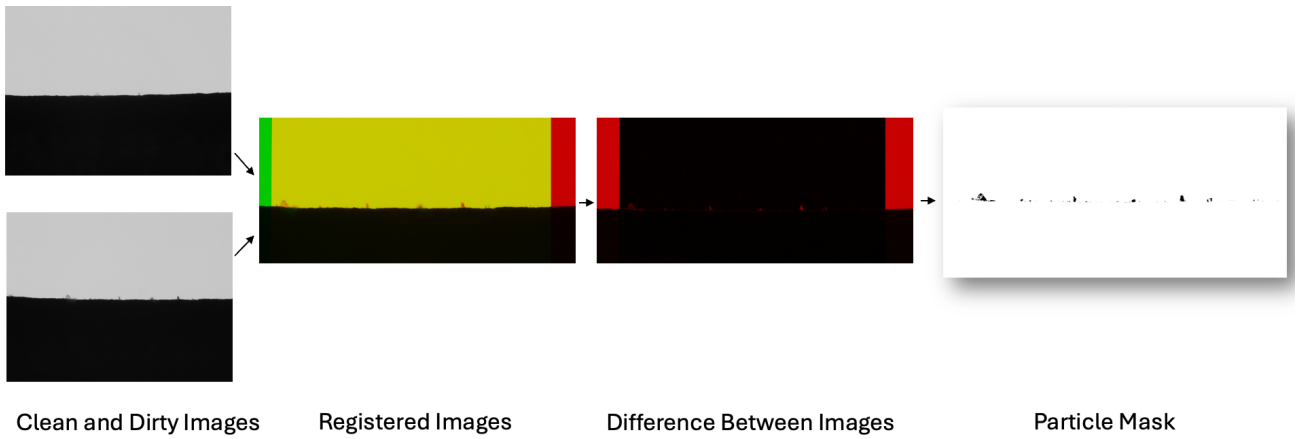


Figure 5: Image processing workflow for edge contamination analysis. Shows the progression from clean and dirty images through registration, difference calculation, to final particle mask generation.

3.3.2 Particle Detection and Qualification

Difference images underwent automated particle detection with edge-specific qualification:

1. **Threshold application:** A threshold of 60 (8 bit scale) was applied to difference images to isolate particle features
2. **Particle analysis:** Standard ImageJ particle analysis measured area, centroid position, and bounding box dimensions for each detected particle
3. **Edge qualification:** Each particle was classified as "edge-associated" if any portion of its bounding box intersected with the extracted edge coordinates
4. **Validation:** Particle measurements were verified for completeness and accuracy, with comprehensive error checking and logging

3.4 The Surface Line Model

The surface-to-edge model, developed by McKeithen et al.,[1] predicts the distribution of particles overhanging an edge by treating the edge as a line drawn randomly across a contaminated surface. The model calculates the expected number of edge particles per unit length based on the surface particle distribution and average particle height.

The key relationship is given by:

$$n_{\text{edge}}(A) = n_{\text{surf}}(A) \times \bar{h}(A) \tag{1}$$

where $n_{\text{edge}}(A)$ is the number of particles per unit edge length with area A, $n_{\text{surf}}(A)$ is the number of particles per unit surface area, and $\bar{h}(A)$ is the average particle height for particles of area A.

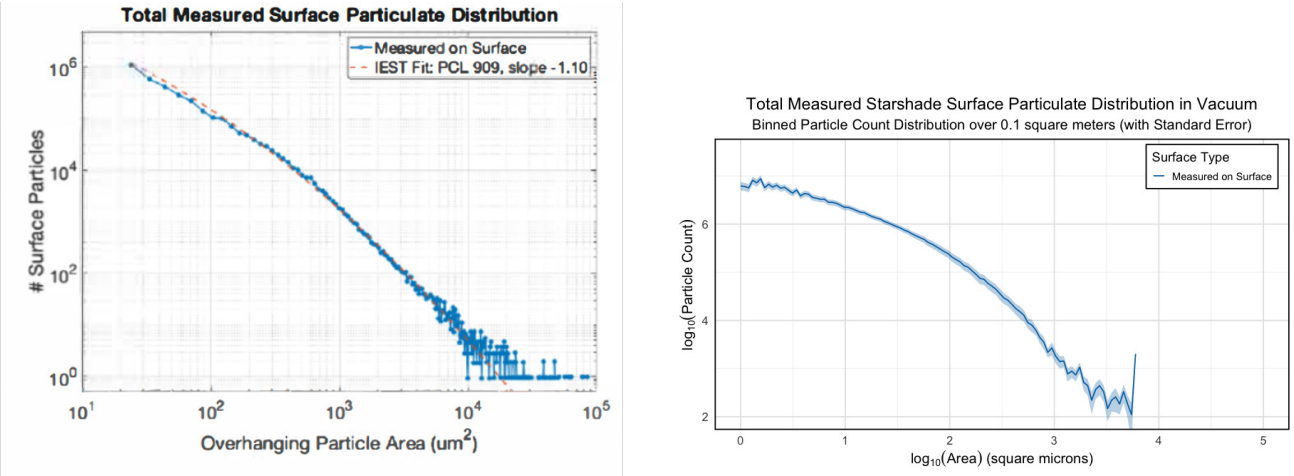
For a complete derivation and detailed explanation of the model assumptions, see McKeithen et al.[1] In our work, we apply this established model to low-vacuum conditions to determine if environmental factors affect the surface-to-edge relationship.

4. RESULTS

We performed several contamination experiments in low vacuum conditions (85 mTorr) to characterize particulate distributions on both starshade edges and calibration mask samples. Our results demonstrate that while surface contamination patterns remain largely consistent across pressure environments, edge contamination behavior shows significant environment-dependent variations that require modifications to existing atmospheric-based models.

4.1 Surface Contamination Results

Figure 6 shows the surface particulate distributions comparing McKeithen et al.'s atmospheric results with our vacuum measurements. Both distributions follow similar relationships when plotted on log-log scales, demonstrating that surface contamination remains largely pressure-independent.



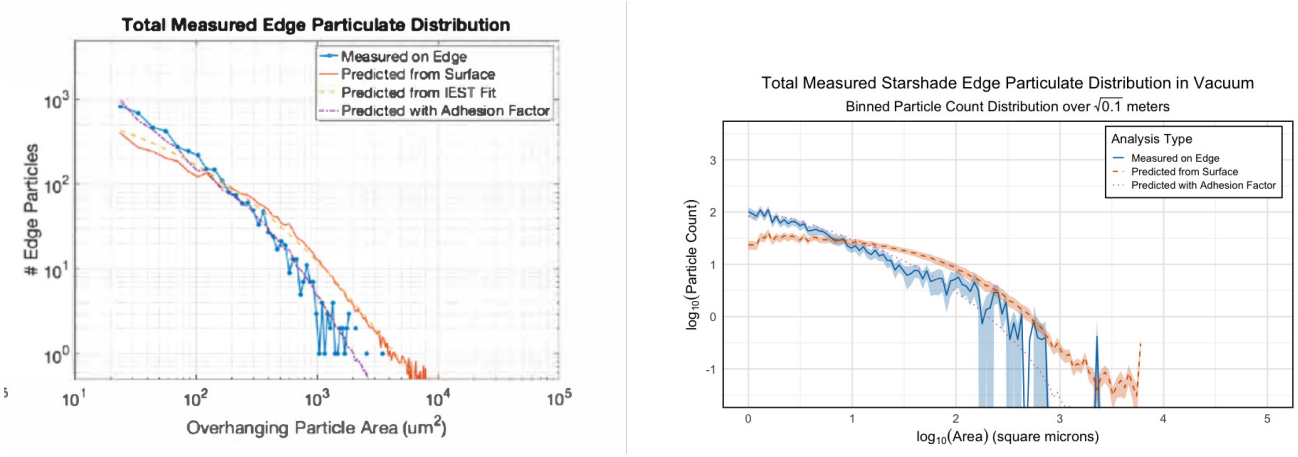
(a) McKeithen et al. atmospheric surface results (b) Vacuum (85 mTorr) surface results

Figure 6: Surface particulate distribution comparison between (a) atmospheric conditions (McKeithen et al.) and (b) vacuum conditions (85 mTorr). The consistent distributions validate that surface contamination physics remain largely pressure-independent.

This surface consistency validates the use of surface-based contamination measurements across different pressure environments and provides confidence in applying the surface line model to vacuum conditions.

4.2 Edge Contamination Results — Critical Discovery

We observed behavior consistent with McKeithen et al.'s atmospheric experiments but with important differences in the adhesion characteristics. Figure 7 presents a direct comparison between atmospheric and vacuum edge particulate distributions.



(a) McKeithen et al. atmospheric edge results

(b) Vacuum (85 mTorr) edge results

Figure 7: Edge particulate distribution comparison between (a) atmospheric conditions (McKeithen et al.) and (b) vacuum conditions (85 mTorr). Note the shift in crossover behavior between the two environments.

Key Finding: Our analysis reveals that the adhesion factor in vacuum follows a n/diameter relationship similar to atmospheric pressure, but with a different crossover point where the distributions intersect—shifting from approximately 14 µm in atmospheric conditions to approximately 3 µm in vacuum conditions.

4.3 Calibration Confirmation

Figure 8 shows the particulate distribution measurements and surface line model application for the calibration mask edge. The calibration mask served as our validation control, using a chrome-on-sodalime glass edge geometry similar to the starshade edge coupons.

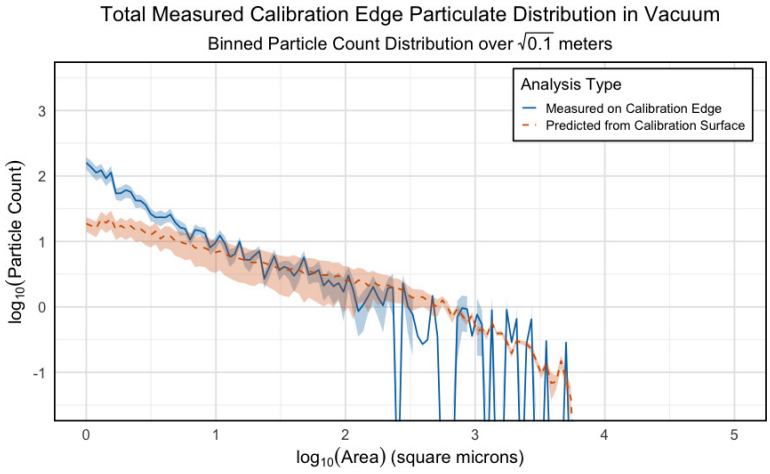


Figure 8: Calibration mask edge particulate distribution in vacuum (85 mTorr). The chrome-on-glass edge provides validation of the surface line model for particles above 10 µm^2 area, which dominate solar glint contributions.

Model Validation in the Critical Size Range: For particles with areas greater than 10 µm^2 (corresponding to diameters 3.6 µm), the calibration mask data demonstrates close agreement between measured edge contamination and surface line model predictions. This agreement is important because particles in this size range dominate solar glint effects that could compromise exoplanet detection.

Confirmation of Methodology: The calibration results validate that our experimental approach and image processing methodology correctly capture the behavior of relevant particles. The surface line model, when applied to the calibration mask, accurately predicts edge contamination for the particle sizes that matter for starshade performance.

Small Particle Regime Limitations: Below 10 µm^2, both the calibration mask and starshade edge data show significant deviations from the surface line model predictions. However, McKeithen et al.'s atmospheric study did not extend into this size range. The behavior we observe in this regime—for both our vacuum data and the calibration mask—requires further investigation.

The calibration confirmation demonstrates that our vacuum contamination methodology produces reliable results for the particle size range important to starshade performance. The agreement between model and measurement for particles above 10 µm^2 provides confidence that the surface-to-edge relationship can be accurately applied to contamination control requirements, while highlighting the need for future studies to characterize small particle adhesion mechanisms under both vacuum and atmospheric conditions.

4.4 Model Performance Analysis and Comparison

Figure 9 presents the relationship between particle area distribution and various model predictions with different adhesion factors, while Figure 10 quantitatively compares total particle area predictions across different model configurations. Together, these analyses reveal that there is no single adhesion factor that optimally predicts all aspects of edge contamination in our low vacuum experiment.

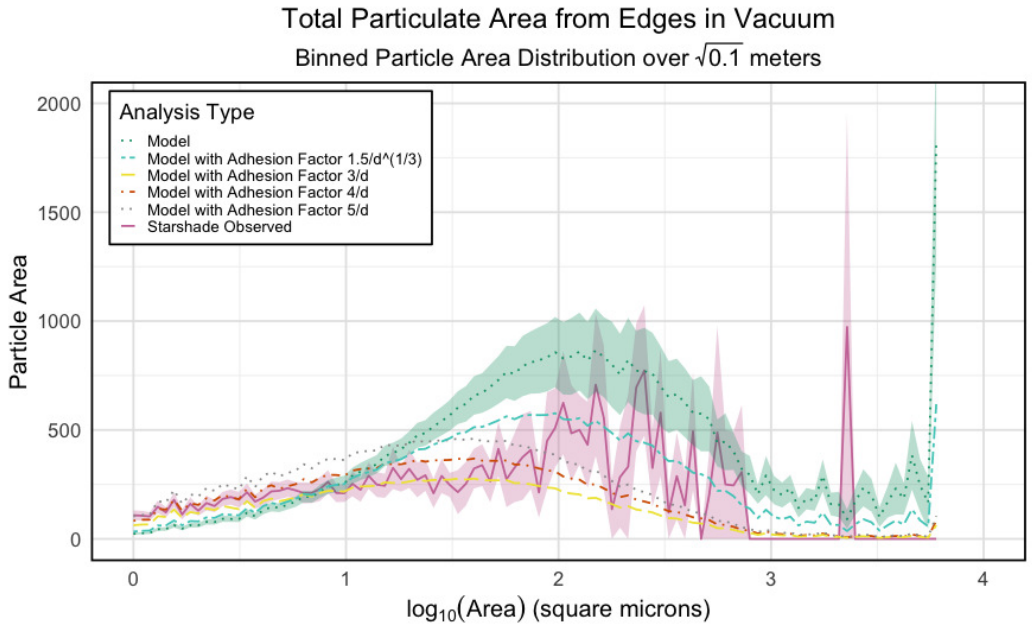


Figure 9: Relationship between particle area distribution and various model predictions with extended adhesion factors. The total particulate area directly determines scatter intensity.

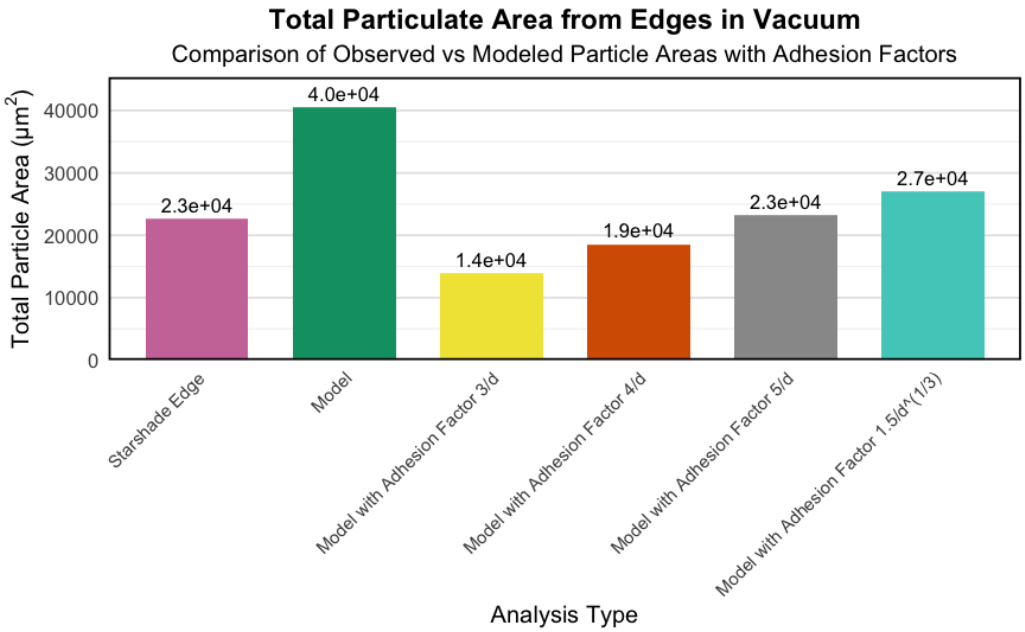


Figure 10: Quantitative comparison of total particle area predictions across eight model configurations showing the necessity of environment-specific adhesion factors.

4.4.1 Parameter-Dependent Model Performance:

The surface line model (green) significantly overestimates total particle area, predicting approximately 40 000 µm^2 compared to the observed ∼23 000 µm^2. This is important because the scattered light will be proportional to the edge particulate area. For calibration between area and scatter, see McKeithen et al. We experimented with multiple adhesion factors and we see that different factors excel at different metrics:

- Total Area Prediction: The $5/d$ adhesion factor provides excellent agreement with observed total contamination area (∼23 000 µm^2 to 24 000 µm^2), making it suitable for overall scatter intensity predictions important to mission planning
- Distribution Shape Fidelity: The $1/d^{1/3}$ adhesion factor better captures the actual particle size distribution, particularly the dominant contribution from medium-sized particles (100 µm^2 to 1000 µm^2)

4.4.2 Implications for Contamination Control:

The convergence of different models on similar total scatter predictions while representing different underlying physics presents both opportunities and challenges. Mission planners can achieve reasonable scatter estimates using simplified factors, but targeted contamination control strategies require more sophisticated models that accurately represent the physical mechanisms governing particle adhesion.

4.4.3 Need for Advanced Modeling:

These results demonstrate that our current simplistic adhesion factors, while useful for specific predictions, cannot capture the full complexity of particle-edge interactions in vacuum environments. Future work must focus on developing physics-based models that incorporate multiple adhesion mechanisms to provide unified predictions across all relevant contamination parameters.

5. DISCUSSION

The shift in the crossover diameter from 14 µm at atmospheric pressure to 3 µm in vacuum suggests that the balance between adhesive and gravitational forces is significantly altered in low-pressure environments. While the crossover point is different, we observed a similar 'adhesion factor' to McKeithen et al.'s experiment. However, our adhesion factor was slightly different, suggesting that the adhesion factor could be pressure dependent. McKeithen et al. suggested that the differences in distribution were likely electrostatic in nature, which could still be the case. However, there are numerous adhesion forces that may be influencing the particle distribution on the edge. Tribble et al. noted that, between a 1 μm glass sphere and a silicon wafer in an atmospheric environment, the adhesion forces would be composed of 71% capillary forces, 22% electrostatic forces, 7% London van der Waals forces, and 1% electrostatic image forces.[2] Capillary forces in this case are likely to be reduced from the low-vacuum environment, as any capillary bridges would evaporate and be pumped out of the chamber by the roughing pump. Therefore, the forces that remain are long-range forces, such as the electrostatic forces to pull the particles to the edges, mechanical interlocking of the dust to the edge, and van der Waals forces to cause the particulates to stick after they make contact with the edge.

Insulating dust particles could exhibit electrostatic discharge when close to surfaces at low vacuum due to Paschen's law. Paschen's law is typically used for the electrical discharge between two electrodes to ignite a plasma.[3] Near low vacuum, there is a significant decrease in the voltage required to ignite a plasma. This breakdown voltage may be able to be applied to insulators that have a high amount of charge. This application has previously been shown with spacecraft charged by dust or ice.[4] In this case, the dust and the starshade edge would both be treated as electrodes. As the charged dust approaches the starshade edge, which would be electrostatically attracted to the edge due to the higher density of electric field lines near sharp edges, the charge might discharge and affect the trajectory of the dust. The change between atmospheric to low vacuum may account for the changes we observe between McKeithen et al.'s work and our work.

Airflow around the dust may influence the particles. In air, the particles settle onto the starshade edge after being sprayed by the atomizer.[1] In vacuum, however, puffing the dust may have an effect on the particulate fallout, as the air would quickly enter the vacuum chamber. Determining the effect of particulate settling is complex and will require more research in order to determine how the flow of the particulates would interact with any electrostatics of the chamber. In future research, we will match the theory we discussed in this section with the experiments and determine the modified particle velocity distributions during the contamination process.

6. CONCLUSION

We investigated the effect of low-vacuum environments on particulate contamination near starshade edges, finding that while surface contamination remains consistent across pressure environments, edge contamination behavior shows significant environment-dependent variations. The adhesion factor follows a similar $1/d$ relationship in both atmospheric and vacuum conditions but with a shift in the balance point from 14 µm to 3 µm diameter.

These findings have important implications for starshade missions, particularly during the launch phase when fairing venting creates low-vacuum conditions similar to our experimental setup. Our results provide the first quantitative validation that atmospheric-based contamination models can be adapted for vacuum conditions with appropriate environment-specific adhesion factors.

Future work should investigate contamination behavior at high vacuum conditions (10^{-6} mTorr)that are more representative of the space environment, test different edge materials and coatings, and explore the use of alternative contaminants such as lunar or Martian simulants.

ACKNOWLEDGMENTS

We thank Dylan McKeithen at JPL for providing the etched samples and calibration wafer used in this work, as well as for the foundational atmospheric pressure study. We appreciate John Ellsworth for helping create the vacuum chamber. We thank Dr. James Hamilton at Photonic Cleaning Technologies for providing the First Contact® Gold formulation that was used to clean the samples. We acknowledge BYU's Department of Mechanical Engineering Project Support Center for the use of the Keyence-VHX 7000 microscope. This research

was funded by the College of Computational, Mathematical, and Physical Sciences as well as the Department of Physics and Astronomy at BYU.

REFERENCES

[1] McKeithen, D., Shaklan, S. B., and Vawdrey, J., "Particulate contamination on starshade optical edges," *Techniques and Instrumentation for Detection of Exoplanets XI*, **12680**, 38 (2023).

[2] Tribble, A. C., Boyadijian, B., Davis, J., Haffner, J., and McCullough, E., "Contamination Control Engineering Design Guidelines for the Aerospace Community," NASA Technical Reports, Rockwell International Corporation (1996). https://ntrs.nasa.gov/api/citations/19960044619/downloads/19960044619.pdf

[3] Paschen, F., "Ueber die zum Funkenübergang in Luft, Wasserstoff und Kohlensäure bei verschiedenen Drucken erforderliche Potentialdifferenz," *Ann. Phys.* **273**, 69–96 (1889). https://doi.org/10.1002/andp.18892730505

[4] Hogue, M. D., Cox, R. E., Mulligan, J., Ahmed, K., Wilson, J. G., and Calle, L. M., "Dynamic gas flow effects on the ESD of aerospace vehicle surfaces," *Journal of Electrostatics* **91**, 21–27 (2018). https://doi.org/10.1016/j.elstat.2017.12.001

[5] Schindelin, J., Arganda-Carreras, I., Frise, E., Kaynig, V., Longair, M., Pietzsch, T., Preibisch, S., Rueden, C., Saalfeld, S., Schmid, B., Tinevez, J.-Y., White, D. J., Hartenstein, V., Eliceiri, K., Tomancak, P., and Cardona, A., "Fiji: an open-source platform for biological-image analysis," *Nature Methods* **9**(7), 676–682 (2012). https://doi.org/10.1038/nmeth.2019